MSAS – Final project

Al Naber Alex Yousef, Balossi Claudia, Corradetti Mario

1 The real system

The Lunar Meteoroid Impact Observer is a CubeSat mission whose aim is to study meteoroid impacts by detecting their flashes on the lunar farside, enabling a more accurate characterization of the lunar meteoroid flux as well as their size, velocity and distribution. The operative orbit of LUMIO is a quasi-halo at Earth-Moon L2 point, and the CubeSat alternates between Science Mode and Navigation and Engineering Mode every halo period.

The main satellite structure is a COTS-based 12U CubeSat produced by ISIS-space [3], complemented by four deployable solar panels, each one covered by a 4 by 4 matrix of AzurSpace 3G30C solar cells [4]. The main payload of the satellite is the LUMIO-cam, that has the aim of detecting the light flashes produced by the meteroids on the lunar far-side. The main goal of this study is to develop a model for the Solar Array Drive Assembly of LUMIO, that moves the solar arrays in order to properly follow the sun by means of a hybrid stepper motor. The configuration of LUMIO is shown in Fig. 1.

In nominal conditions the LUMIO-cam has to point towards the Moon while the SADA keeps the solar panels orthogonal to the direction of the Sun, with a maximum shift of $\theta = \pm 4.5°$. For a better overview of the system behavior, this study also considers the response in the off-nominal condition of a solar array failure after 20 days.

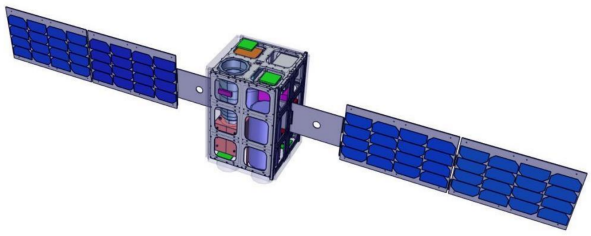

Figure 1: LUMIO configuration.

2 The physical model

2.1 Orbital Mechanics

The trajectory of LUMIO in Earth Equatorial Inertial reference frame has been provided over 40 days, while the Earth trajectory (in Sun-centred Ecliptic frame) as well as the Moon path around the Earth have been computed from ephemeris. In order to ease the definition of the attitude of the satellite the position vector of the Earth has been rotated around the X-axis by the angle ε (obliquity of the ecliptic), projecting it onto the equatorial plane.
In order to check if the satellite is in eclipse with respect to the Moon and the Earth a cylindrical model for the sun rays has been considered due to the high distance between LUMIO and Sun.

2.2 Hybrid Stepper Motor

The Hybrid Stepper Motor governing the movement of the solar arrays is composed by a permanent magnet rotor connected to a shaft and a stator which is surrounded by windings connected

to a DC source. The one implemented in LUMIO's SADA is a two-phase HSM: the stator has been modeled by means of two RL circuits (see Fig. 2), where the resistor represents the resistance given by the coils and the inductor models the magnetic field produced by the windings.

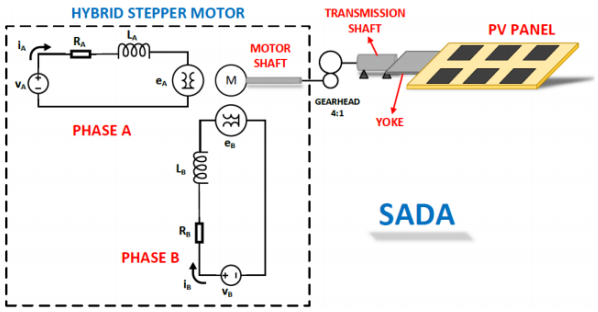

Figure 2: Hybrid Stepper Motor model [1]

The rotor can instead be modeled as a gear with a number of teeth that can be computed from Eq. (1), where $\theta_{step} = 18°$ is the given step angle of the motor and $N = 4$ is the number of stator phases.

$$p = \frac{360°}{\theta_{step} N} = 5 \tag{1}$$

The interaction of the magnetic material of the stator pole with the permanent magnet causes a detent torque that is here neglected since it's contribution is much smaller than the other torques acting on the motor ([2]). Panels and yoke have been modeled as thin rectangular plates of given dimensions and their inertia has been computed as $J = \frac{mL^2}{12}$, where m is the mass of the plate and L its length in the direction normal to the rotation axis. Finally, the transmission system considers the inertia of the shaft (assumed as $J = 4.5 \times 10^{-5}$ Kgm^2, from [2]) and a reduction gear of 4:1 from the motor shaft to the solar arrays.

2.3 Thermal Analysis

With the purpose of carrying out a preliminary thermal analysis, it is only considered the CubeSat frame made by Aluminum 6061 T6 (both for the body and the panels). The body of the spacecraft is covered in a spray paint made up of 48% aluminum, 27% gold and 25% silvered teflon. Regarding the panels, it is considered that each of them contains 16 solar cells of area $A_{SC} = 26.51$ cm^2 [1], and that the efficiency of these cells is 30%. This value will be directly subtracted from the absorptivity of the cells in the thermal balance. The optical and the thermal properties of the materials are shown in Table 2.

The only incoming radiation considered in this thermal analysis is the one coming from the Sun. Therefore, the radiation produced and reflected (albedo) by the Moon and the Earth is neglected. In the thermal balance, for each surface of the CubeSat it is only considered the perpendicular component of the incoming radiation.

The heat sources considered for the thermal balance are the power dissipated by the internal components (that will be a percentage of the total power of the components) $P_{diss} = 3.36$ W, and the power produced by the heater $P_{heat} = 15$ W [4]. The latter prevents critical components from dropping below the minimum working temperature threshold.

In order to simplify the analysis, a lumped-parameter approach is adopted. It was decided to use one lump for each surface (then 6 for the body and 4 for the panels) as shown in Fig. 3. This approach is valid whenever the heat conduction within the surface is much faster than heat transfer across its boundary. Since the surfaces are pretty small and the Al 6061 T6 has a good conductivity, that approach could be considered a good approximation.

[1] Fig. 2 is taken from assignment presentation notes

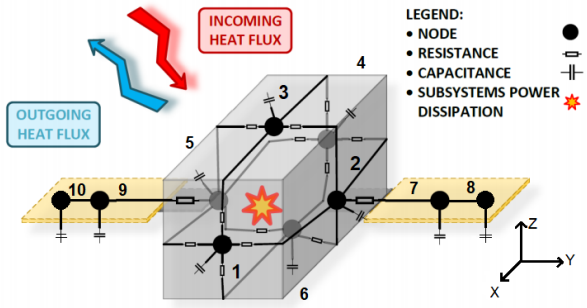

Figure 3: Nodes definition

3 The mathematical model

3.1 Orbital Mechanics

The attitude of LUMIO has been determined considering that the LUMIO-cam has to continuously point to the Moon. Thus, the X vector of the satellite reference frame can be computed as Eq. (2a). The Y axis points in the direction of the normal to the plane containing Lumio, Moon and Sun (Eq. (2b)) and the Z axis completes the set (Eq. (2c)).

$$\begin{cases} \mathbf{X}_{\text{LUMIO}} = \dfrac{\mathbf{R}_{\text{LUMIO @ moon}}}{\text{R}_{\text{LUMIO @ moon}}} & \text{(2a)} \\ \mathbf{Y}_{\text{LUMIO}} = \dfrac{\mathbf{X}_{\text{LUMIO}} \wedge \mathbf{R}_{\text{LUMIO @ Sun}}}{\text{R}_{\text{LUMIO @ Sun}}} & \text{(2b)} \\ \mathbf{Z}_{\text{LUMIO}} = \mathbf{X}_{\text{LUMIO}} \wedge \mathbf{Y}_{\text{LUMIO}} & \text{(2c)} \end{cases}$$

The vector position of the Sun in LUMIO's reference frame has been computed through to the attitude transformation matrix in Eq. (3), considering that $\mathbf{R}_{\text{Sun @ LUMIO}} = \mathbf{A}_{SL}^{\text{T}} \mathbf{R}_{\text{LUMIO @ Sun}}$

$$\mathbf{A}_{SL} = [\mathbf{X}_{\text{LUMIO}} \mid \mathbf{Y}_{\text{LUMIO}} \mid \mathbf{Z}_{\text{LUMIO}}] \tag{3}$$

Since the solar arrays have to move according to the direction of the Sun, it is useful to determine the angle of the panels with respect to the Sun rays θ as

$$\theta = \arctan \frac{\mathbf{R}_{\text{Sun}}|_x}{\mathbf{R}_{\text{Sun}}|_z} \tag{4}$$

where the notation $\mathbf{R}_{\text{Sun}} = \mathbf{R}_{\text{Sun @ LUMIO}}$ has been used for simplicity. θ is measured counterclockwise from the Z axis.

Moreover, the normal to each face of the CubeSat main body has been defined following the numbering shown in Fig. 3. The incidence angle of the Sun rays on the six faces has been computed as the angle between the normal to the surfaces and the direction of the Sun as seen from LUMIO.

3.2 Hybrid Stepper Motor

The mathematical model that describes the dynamics of the hybrid stepper motor can be derived starting from a torque balance equation:

$$J\dot{\omega} + T_L = T_e - B\omega \tag{5}$$

In Eq. (5), the total electromagnetic torque generated by the windings of the stepper motor can be described as

$$T_e = -I_a N_r b_{EMF} \sin(N_r\theta) + I_b N_r b_{EMF} \cos(N_r\theta) \tag{6}$$

while the torque load considers the contribution of the external masses connected to the transmission:

$$T_L = \frac{1}{\tau}(J_{sp} + J_y)\dot{\omega} \tag{7}$$

In these equations, I_a, I_b are the currents in phases A and B respectively, N_r is the number of rotor's teeth, b_{EMF} represents the back Electromotive Force, J, J_{sp} and J_y are respectively the inertia of rotor, solar panel and yoke.
Moreover the term Bω, that account for viscous friction, has been considered, where the coefficient $B = 8 \times 10^{-5}$ Nms/rad has been derived from [2].
Substituting Eq. (6) and Eq. (7) into the torque balance yields Eq. (8c).

Eq. (8a) and Eq. (8b) can be instead derived from the Kirchhoff Voltage Law across the two phases circuit, considering the voltage source of the two phases, the voltage drop across the resistors and the contribution of the electromotive torque.

Finally, Eq. (8d) yields the rotor angular displacement θ.

$$\begin{cases} \dot{I}_a = \dfrac{1}{L}\left(V_a - RI_a + \omega N_r b_{EMF} \sin N_r\theta\right) & \text{(8a)} \\ \dot{I}_b = \dfrac{1}{L}\left(V_b - RI_b - \omega N_r b_{EMF} \cos N_r\theta\right) & \text{(8b)} \\ \dot{\omega} = \dfrac{1}{J + \frac{1}{\tau}(J_{sp} + J_y)}(T_e - B\omega) & \text{(8c)} \\ \dot{\theta} = \omega & \text{(8d)} \end{cases}$$

3.3 Thermal Analysis

The general conduction equation can be obtained from the conservation of energy for *closed systems* (Eq. (9))

$$\frac{d}{d\tau}\iiint_V u\rho dV = \iint_S \dot{\mathbf{Q}}'' \cdot \mathbf{n} dS + \iiint_V \dot{U}''' dV \tag{9}$$

that can be rewritten as in Eq. (10)

$$\rho c V \frac{\partial T}{\partial \tau} = \Sigma\dot{Q} + \dot{U} \tag{10}$$

where $\Sigma\dot{\mathbf{Q}}$ is the sum of all heat fluxes taken with their sign and $\dot{U}$ is the possible source or sink of heat. Recalling that the heat fluxes between two close surfaces can be written as

$$\dot{Q}_{i\to j} = \frac{1}{R_{i\to j}}(T_i - T_j) \tag{11}$$

where the thermal resistance $R_{i\to j}$ between two nodes is the sum of the resistances across each surface included in the node. The latter has the following expression

$$R = \frac{a}{k\ b\ t} \tag{12}$$

where a is the dimension along which the resistance is considered, b is the perpendicular dimension, t is the surface thickness and k is the conductivity. Putting together Eq. (10),Eq. (11) and Eq. (12), and writing the thermal balance for node 1,2,7 and 8 (since the others have the same expression), we obtain the system of equation summarized below, where the index *sc* and *sp* refer respectively to solar cells and solar panels, and θ is the angle between the normal to the surface and the incident radiation.

$$
\begin{cases}
\dot{Q}_1 = E_s \alpha_1 A_1 cos(\theta_1) - \epsilon_1 A_1 \sigma T_1^4 \\
\dot{T}_1 = \dfrac{1}{\rho_{Al} c_{Al} V_1} \left(\dfrac{(T_2 - T_1)}{R_{1\to2}} + \dfrac{(T_3 - T_1)}{R_{1\to3}} + \dfrac{(T_5 - T_1)}{R_{1\to5}} + \dfrac{(T_6 - T_1)}{R_{1\to6}} + \dot{Q}_1 + \dot{U}_{power} \right) \\
\dot{Q}_2 = E_s \alpha_2 A_2 cos(\theta_2) - \epsilon_2 A_2 \sigma T_2^4 \\
\dot{T}_2 = \dfrac{1}{\rho_{Al} c_{Al} V_2} \left(\dfrac{(T_1 - T_2)}{R_{1\to2}} + \dfrac{(T_3 - T_2)}{R_{2\to3}} + \dfrac{(T_4 - T_2)}{R_{2\to4}} + \dfrac{(T_6 - T_2)}{R_{2\to6}} + \dfrac{(T_7 - T_2)}{R_{2\to7}} + \dot{Q}_2 + \dot{U}_{power} \right) \\
... \\
\dot{Q}_7 = E_s(((\alpha_{sc} - \eta_{sc}) A_{sp} + \alpha_{Al}(A_{sp} - A_{sc})) cos(\theta_{7-front}) + \alpha_{back} A_{sp} cos(\theta_{7-back}))) + \\
\quad -(\epsilon_{sc} A_{sc} + \epsilon_{Al}(A_{sp} - A_{sc}) + \epsilon_{back} A_{sp}) \sigma T_7^4 \\
\dot{T}_7 = \dfrac{1}{\rho_{Al} c_{Al} V_7} \left(\dfrac{(T_2 - T_7)}{R_{2\to7}} + \dfrac{(T_8 - T_7)}{R_{7\to8}} + \dot{Q}_7 \right) \\
\dot{Q}_8 = E_s(((\alpha_{sc} - \eta_{sc}) A_{sp} + \alpha_{Al}(A_{sp} - A_{sc})) cos(\theta_{8-front}) + \alpha_{back} A_{sp} cos(\theta_{8-back}))) + \\
\quad -(\epsilon_{sc} A_{sc} + \epsilon_{Al}(A_{sp} - A_{sc}) + \epsilon_{back} A_{sp}) \sigma T_8^4 \\
\dot{T}_8 = \dfrac{1}{\rho_{Al} c_{Al} V_8} \left(\dfrac{(T_7 - T_8)}{R_{7\to8}} + \dot{Q}_8 \right) \\
...
\end{cases}
$$

Integrating this system of equation, the temperature profile for each node is obtained.

4 Numerical integration

4.1 Hybrid Stepper Motor

A preliminary analysis on the eigenvalues of the system has been considered in order to choose the most suitable integration scheme, starting from the state space realization of the differential equations. The initial conditions have been considered as reference ($\theta = 0$ °), and the resulting eigenvalues are $\lambda_{i,mech}$ = (-6800, -6221.9, -578.18, 0), $i = 1, 2, 3, 4$.
The system is therefore stable ($\mathrm{Re}(\lambda_i) < 0$) but it shows a stiff behavior, thus the integration scheme has to be chosen accordingly. As a result, the most efficient integrator for the system is ODE 15s.

4.2 Thermal Analysis

The same procedure is followed in order to choose the most suitable integration scheme for the thermal subsystem and the resulting eigenvalues, computed linearizing around the reference condition at T_0, have negative real part with magnitude that span between 0 and -4.5× 10^{-3}. Therefore the system is not stiff and ODE 113, ODE 15s and ODE 23s grant high convergence performances.

Table 1 summarizes the integration time for several schemes, considering a fixed relative tolerance of 10^{-7} for the mechanical system and 10^{-13} for the thermal part.

Table 1: Time requested by different ODEs

System	ODE 15s	ODE 23s	ODE 23t	ODE 23tb	ODE 113
Mechanical	3.778743 s	7.023357 s	5.098844 s	5.990903 s	-
Thermal	4.360684 s	75.709221 s	7.110199 s	12.816633 s	7.446849 s

5 The simulation framework

The workflow followed in the project is summarized in Fig. 4.

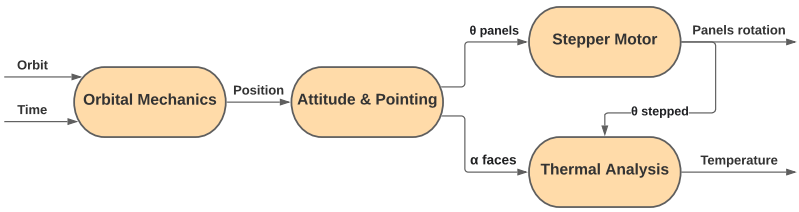

Figure 4: Project flowchart

1. *Orbital Mechanics*: the block takes as input the given orbit and, by considering datas from ephemeris, computes the position of LUMIO with respect to the Moon and Sun.
2. *Attitude and Pointing*: starting from the position vectors, the attitude of LUMIO is retrieved and angle of incidence of the Sun rays on the six faces and the solar arrays is computed. Moreover, a check on the eclipse is performed.
3. *Stepper Motor*: this section takes as inputs the time span of the orbit and the incidence angle of the solar panels with the Sun, and yields the resulting "stepped" angle computed from the integration of the mechanical system's ODEs described in Section 3.2.
4. *Thermal Analysis*: the block considers the incidence angle of the Sun on the six faces of LUMIO and the actual angle of the solar panel extracted from the Stepper Motor block and yields the temperature profiles across the whole time interval.

6 System response

6.1 Orbital Mechanics

The trajectory of LUMIO quasi-halo orbit around L2 is shown in Fig. 5, both from the Moon and Earth point of view.

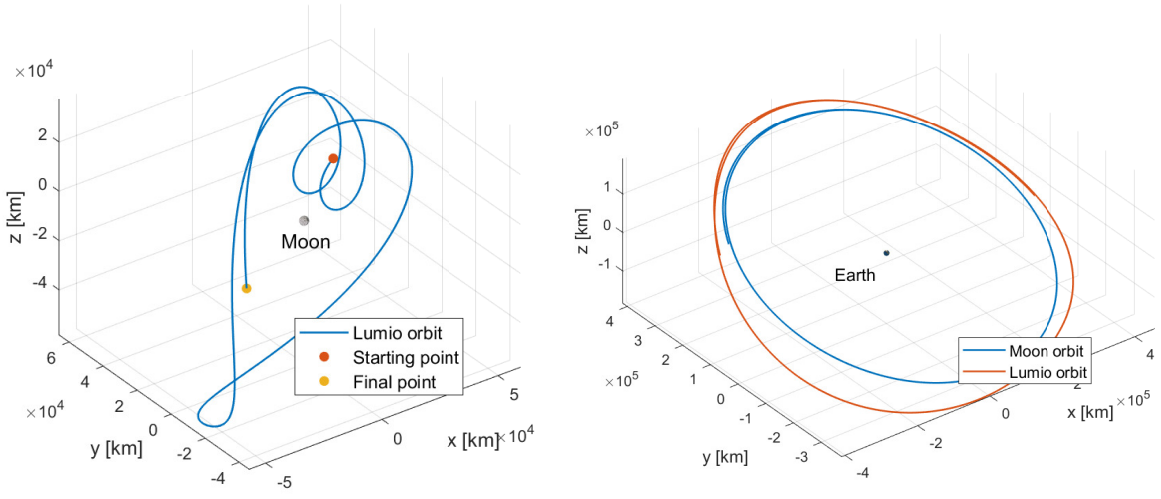

(a) **(b)**

Figure 5: LUMIO orbit as seen from: (a) Moon, (b) Earth

The results of the computation of the incident angle of the Sun rays on the six faces of the CubeSat can be appreciated in figure Fig. 6.

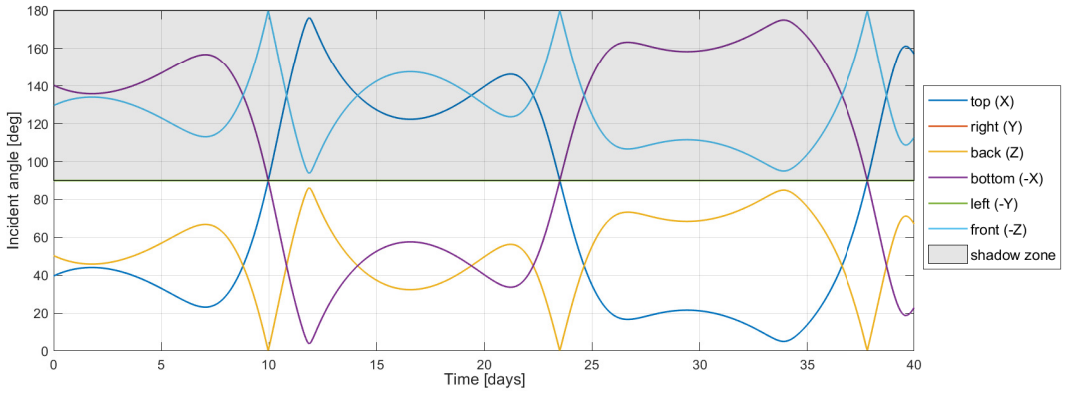

Figure 6: Incident angle on LUMIO's faces

Angles $\alpha < 90°$ (positive and negative angle with respect to the face's normal are considered equivalent), mean that the face is lit, while if $\alpha > 90°$ the face is in shadow.

6.2 Hybrid Stepper Motor

The motor is activated only 130 times during the whole time interval of 40 days, thus the response in terms of current and voltage variation is shown in Fig. 7 considering only the overall operational time of the HSM. It can be seen that every step lasts less than 1 s, and the SADA is required to rotate the panels more or less once every 7 hours, thus the dynamics of the motor can be considered decoupled from the thermal one.

Fig. 7 shows the stator circuits response, in terms of current intensity and voltage. Voltage changes depending on the direction in which the panels have to rotate, switching between 0 V and ± 12 V. The initial condition considers the circuit A switched on, while B is switched off. If the motor has to advance of one step the circuit B has to be switched on, while A is off. The successive forward step can be obtained by switching off again the circuit B and applying an opposite voltage to the circuit A, and so on. The resulting angle (in nominal conditions) is shown in Fig. 8.

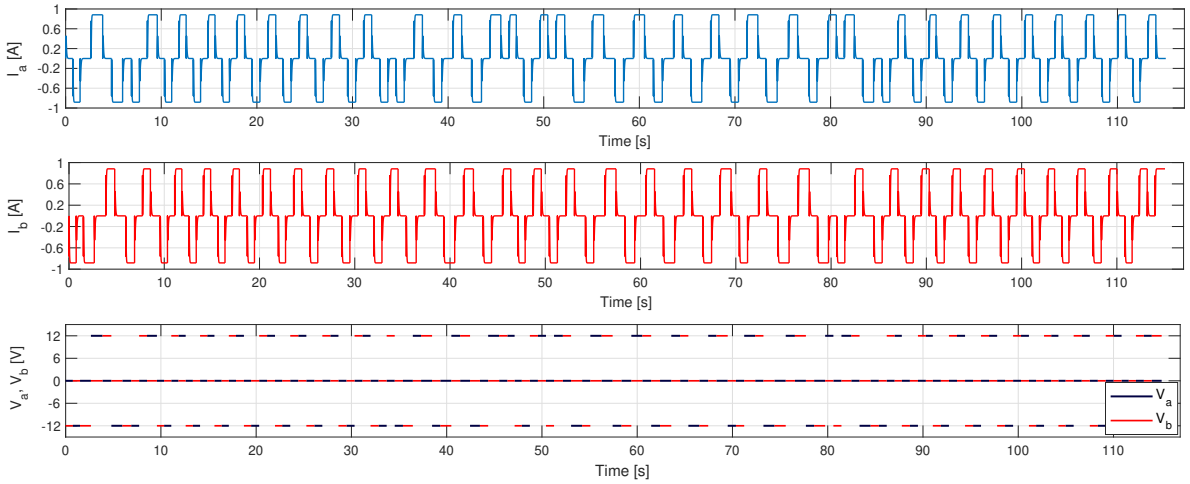

Figure 7: Current intensity and voltage respectively in phase A and phase B

For completeness, a short parametric analysis has been carried out varying the values of R and L of the HSM model.

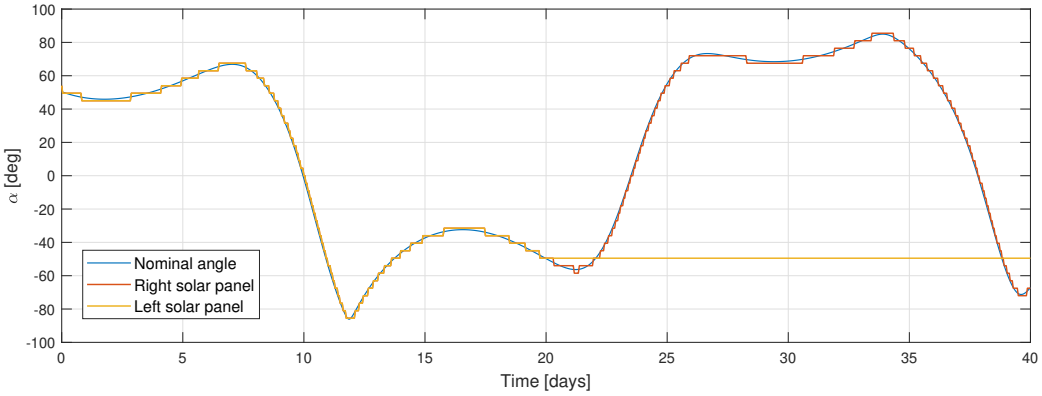

Figure 8: Nominal incident angle of Sun rays on solar panels' surface compared with stepped angle θ provided by the SADA in both nominal and off-nominal conditions

6.3 Thermal Analysis

During the analysis of the thermal response of the system, it has been considered as an assumption that, in nominal conditions, the heater is on only if the temperature of one of the six faces is below the minimum working temperature (T_{min} = -5°, from [4]). In off nominal conditions (one solar panel stops rotating), the heater has been turned on from the instant corresponding to the panel failure. The temperatures reached by the system are shown in Fig. 9 in case of nominal conditions.

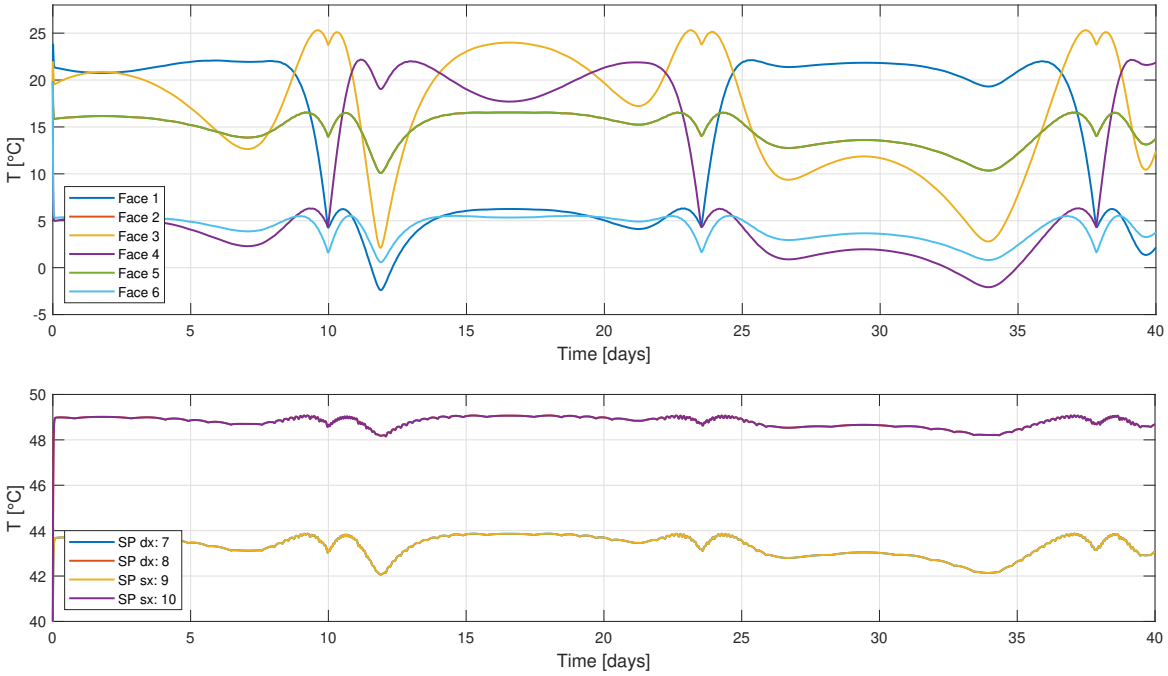

Figure 9: Thermal response in nominal conditions for both LUMIO's faces and solar arrays

In the case of failure of the left solar panel after 20 days the heater is not able to provide enough heat to stay within the operative temperature range, as the broken solar array reaches a minimum of -71° and consequently the adjacent face of the CubeSat has a temperature drop up to -17°.

References

[1] *30% Triple Junction GaAS Solar Cell.* Tech. rep. AZUR SPACE Space Solar Power GMBH, May 2019.

[2] K Balakrishnan, B Umamaheswari, and K Latha. "Estimation of rotor position and speed for Hybrid Stepper Motor under various phase excitation schemes and compensated resonance". In: *Acta Astronautica* (May 2011).

[3] Michele Marino et al. "Innovative Solar Array Drive Assembly for CubeSat Satellite". In: *Conference Paper* (May 2016).

[4] M Topputo F.and Massari et al. "LUMIO: Characterizing lunar meteoroid impacts with a CubeSat." In: *69th International Astronautical Congress* (Oct. 2018).

Appendix

Table 2: Optical and thermal properties of the materials

Material	Absorptivity α	Emissivity ϵ	Conductivity $[\frac{W}{m\ K}]$	Heat capacity $[\frac{J}{kg\ K}]$
Al 6061 T6	0.031	0.039	152	900
Gold	0.3	0.03	-	-
Silvered Teflon	0.163	0.8	-	-
GaAs Solar Cell [1]	0.91	0.8	-	-

Table 3: Solar panel parameters

Symbol	Name	Value	Units
L	Length	$325 \times 10^{-}3$	m
h	Height	$205 \times 10^{-}3$	m
t	Thickness	$5 \times 10^{-}3$	m
m	Mass	0.5	kg
Jsp	Inertia	$1.8 \times 10^{-}3$	kgm^2

Table 4: HSM parameters

Symbol	Name	Value	Units
R	Resistance	13.6	Ω
L	Inductance	2×10^{-3}	H
b_{EMF}	Back$_{EMF}$ amplitude	0.53	Vs
τ	Gear head reduction	4	-
V	Voltage	12	V
B	Viscous friction	8×10^{-5}	N m s rad^{-1}
J_m	Rotor inertia	4.5×10^{-5}	kg m^2

Table 5: Yoke parameters

Symbol	Name	Value	Units
L_y	Length	198×10^{-3}	m
h_y	Height	1×10^{-1}	m
t_y	Thickness	5×10^{-3}	m
m_y	Mass	2.673×10^{3}	kg
J_y	Inertia	2.2275×10^{-4}	kg m^2

Weights ↓	Fail (<18)	Poor (18-21)	Fair (22-25)	Good (26-28)	Excellent (29-30)
Report (50%)	• Major modelling errors (wrong assumptions, missing domains) • Simulation contains several wrong concepts • Report awfully written	• Some modelling errors (assumptions not complete, missing domains) • Simulation part contains several conceptual mistakes • English is poor	• Fair modelling (good assumptions, physics caught) • Simulation not appropriate (wrong integration scheme) • Report not clear, minor issue (typos)	• Detailed modelling (assumptions detailed and justified, all physics considered) • Minor problems with simulation (numerical issues) • Good English	• Accurate modelling (all physics considered, second order effects quantified/modeled) • Good simulation techniques (integrator, numerical issues) • Good English
Code (30%)	• Code does not run • Major algorithmic errors • Code not complete	• Minor algorithmic errors • Code is not documented • Code takes unnecessary long to run (inefficient)	• Code runs smoothly, fairly documented • Computational efficiency improvable	• Code runs smoothly, well documented • Care is taken to computational efficiency • Add-ons are produced	• Code runs smoothly, well documented • Care is taken to computational efficiency • Valuable add-ons are produced
Presentation (20%)	• Major errors in the presentation • Questions are not answered	• Poor presentation • Poor time management • Poor answers to questions	• Fair presentation • Poor time management • Weak answers to questions	• Good presentation • Good management of time • Answers not exhaustive	• Excellent presentation • Excellent time management • Satisfactory answers given

Figure 10: Rubric used for grading.